HISTO-MRI

HISTO - MRI

This project has received funding from the European Union's H2020 Programme under grant agreement no 737180— HISTO-MRI

D5.1: Proof of Concept of New MRI Technology Built

Version	Date	Reviewer
1	07/04/2021	Juan Pablo Rigla

Table of contents

1 Deliverable description

This deliverable describes the implementation of all systems for the new MRI system and the prepolarization system for the HISTO-MRI project.

2 Introduction

In this deliverable we describe the state of the integration of the different components of the HISTO-MRI scanner (Fig.1), as well as the integration of the prepolarization system proposed in this project in the MRI scanner available at Tesoro Imaging S.L. The Grafical User Interface (GUI) developed to control the different components that are part of the diagnostic system of the HSITO-MRI scanner and the prepolarization system is described.

Figure 1: Picture of the HISTO-MRI system.

2.1 HITO – MRI Scanner.

2.1.1 Main Magnet.

For the main magnetic field, B_0, the main requirements to meet for the high resolution targeted in the HISTO – MRI project are a Rampable magnetic field up to 1 T and a spatial homogeneity better than 100 ppm in a FoV defined by a spherical region of diameter 20mm. To meet this goal, we have opted for an electromagnet with a classical “H” – shaped structure. This

magnet has a gap, space free between magnetic poles, of 70 mm and a diameter poles of 250 mm. A profile – height variations <100 µm in the magnetic poles was adopted to achieve adequate homogeneity ,71 ppm in the FoV[1].

To generate the field, the magnet counts with two circular coils of 156 turns each, with a total conductor cross section of 51 mm^2. With this design, a current of ≈ 180 A through the coils results in the desired maximal-field strength of 1 T. With this design the electromagnet has a total mass of 950 kg. A photograph of the main magnet is shown in **Fig.2**.

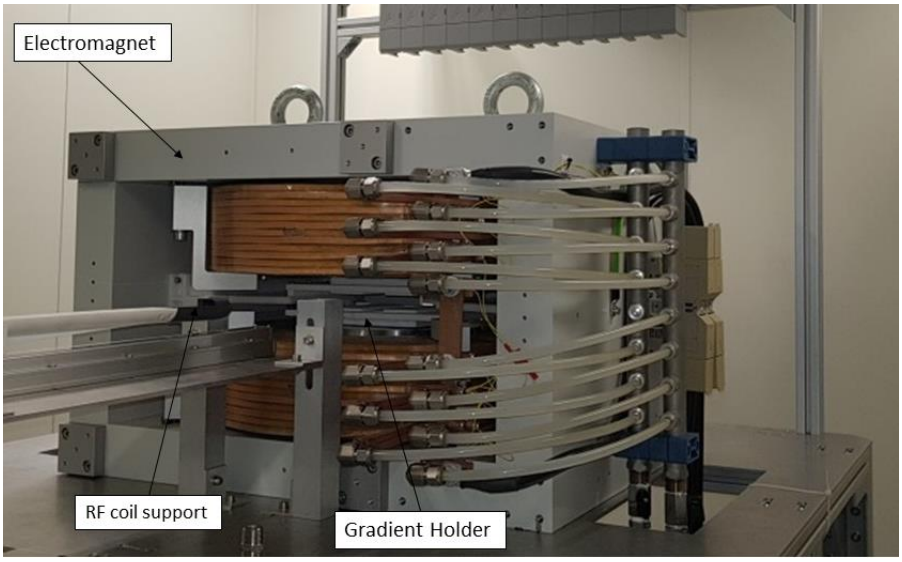

Figure 2: Picture of the main magnet, including the gradient coils and the radio-frequency coil and sample holder, which can be moved in and out of the scanner by means of a stepper motor.

For the generation of the maximum magnetic field, the magnet requires currents up to 180A, leading to voltage drops of up to 30 V across the coils. Hence, up to 5.4 kW of power can be dissipated in the magnet structure. For generate the magnetic field this magnet uses a Danfysik 9100 Unipolar Power Supply. This power supply is a current regulated power supply with a stability of 19 ppm at 200 A.

We have split each coil into four loops, with three layers per loop, to allow for efficient cooling. The thermal simulations that a water flow of 12 l/min and a drop pressure of 4 bar will limit the temperature increase at the coils to 6 K. This magnet uses a SMC HRS060 thermochiller cooling system. Monitoring of the water flow and temperature is realized by two flowmeters (SMC HRS-PF3W540) located at the input and exit of the electromagnet.

We have characterized the spatial field-strength distribution and overall performance of the main magnet with a Hall probe attached to a 3-D positioning system. The positioners in the transverse (vertical) directions move in a range of up to 500 mm and are accurate at the 100 μm level, whereas the Hall probe is specified to have an accuracy of 0.1 mT with the settings used in most measurements. For these tests, we supplied current to the magnet with a Danfysik 9100 Unipolar Power Supply. The magnetic field profile along the Z-axis for 1 T is shown in **Fig.3**.

[1] J. P. Rigla *et al.*, "Low-Field Rampable Magnet for a High-Resolution MRI System," in *IEEE Transactions on Magnetics*, vol. 56, no. 2, pp. 1-7, Feb. 2020, Art no. 5100107. doi: 10.1109/TMAG.2019.2950891

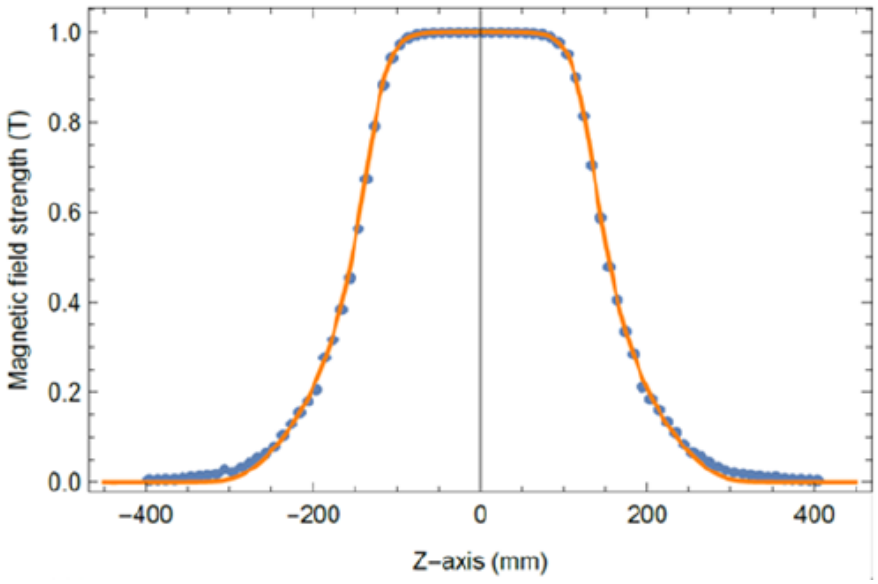

Figure 3: (Top) Magnetic Field profile along the Z-axis for B_0~1 T for COMSOL simulations (solid, orange line) and experimental measurements (blue points).

For the experimental characterization, we scanned a cubic volume of sides 20 mm and we obtained an experimental homogeneity of ≈ 71 ppm, very close to the simulated value (≈ 68 ppm). Deviations from the nominal B_0 along the three Cartesian axes can be read in **Fig.4**.

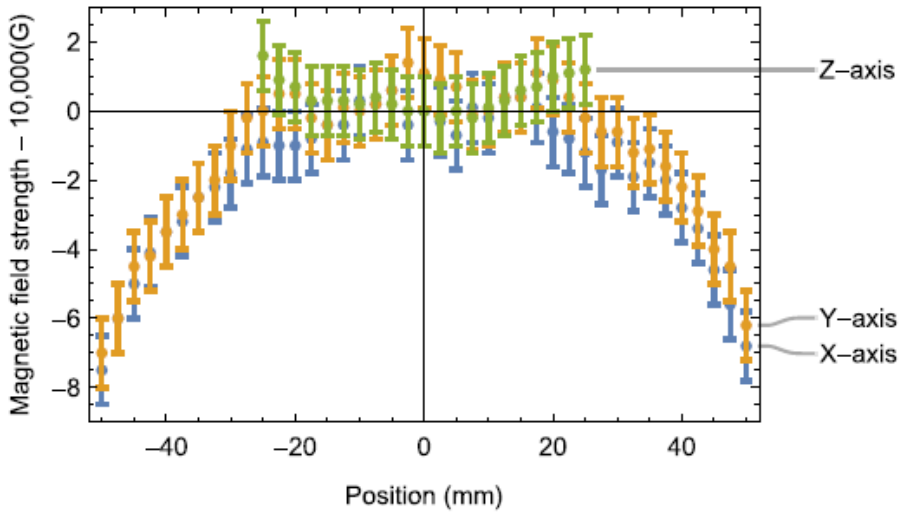

Figure 4: Magnetic-field strength along the *X*- (blue), *Y*- (yellow), and *Z* (green)-axes for $B_0 \approx 1$ *T*.

The weight of the magnet imposes the use of a robust and reliable mechanical structure. To ensure the structural integrity of the system and the building, the load must be kept <350 kg/m2 and the load distribution should be as uniform as possible. To avoid the strong forces between the support structure and the magnet, we built the former out of aluminum 6063. The mechanical structure of the magnet is formed by two components: the magnet table and the load support. A photograph of the electromagnet with the mechanical support mounted in the MRILab at the i3M is shown in **Fig.5**.

Figure 5: Picture of the magnet and the mechanical support structure.

2.1.2 Gradient System.

For the design of the gradient coils, we considered that these coils should have the minimum possible inductance to be able to reach the rise and fall times ≤ 10 μs and the minimum possible resistance to be able to withstand the high currents (<500 A). The magnetic gradient system manufactured has a planar and open configuration and is composed of ten planar coils. The manufacturing the coils was made from a conductive material used is a special OF-OK Copper hollow conductor provided by Luvata. Also, connection hub was designed and manufactured and welded to the gradient coils. The connection hub connects both electric and hydraulic systems with the gradient coils. The dimensions of the selected hollow tube are shown in **Fig.5**. A dielectric structure manufactured by sintering polyamide is used to fix the different gradient coils, see **Fig.5**.

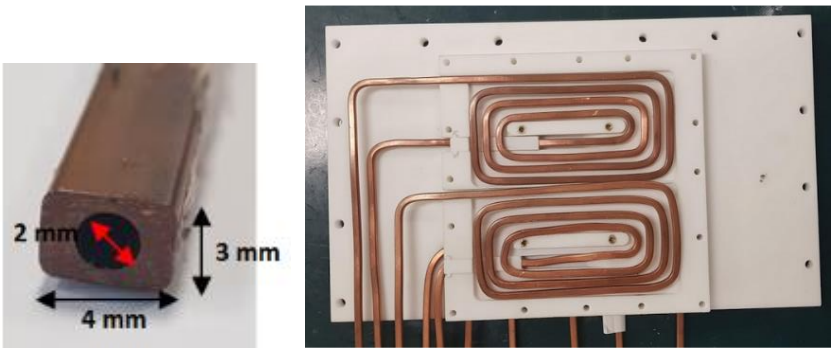

Figure 5: (Right) Cross section hollow tube. (Left) Y gradient coil and gradient polyamide structure

The gradient coils have been magnetically characterized by studying the gradient magnetic field and also the resistance and inductance values at different frequency ranges once built (see **Fig.6, Right**), before installing them inside the main magnet. The expected gradient field by using an intensity current of I = 400 A is G_x = 1.7 T/m. Experimental measurements confirm the performed simulations (**Fig.6, Left**).

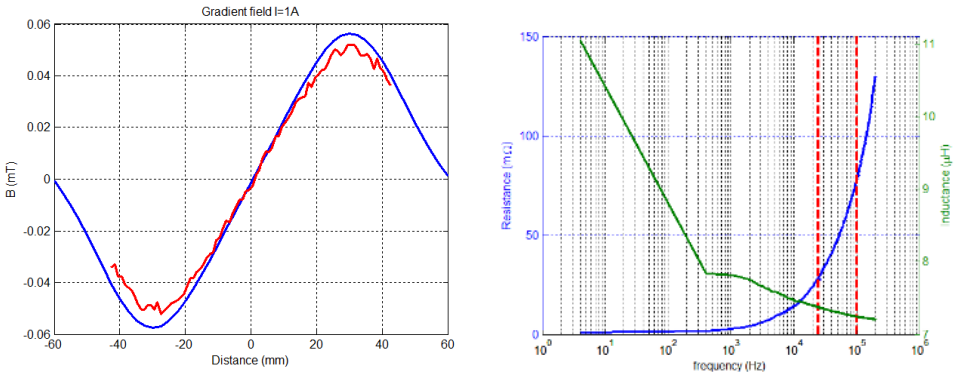

(a) (b)

Figure 6: (Right) Magnetic profile by using an intensity current I=1A. Blue line: expected values, red line: experimental values. (Left) X-coil set axis resistance and inductance experimental values in a frequency range between 4Hz and 200 kHz.

To use a high intensity current, it is necessary to refrigerate each of the coils. This is done using a pump and cooler that provide a constant flow to the entire hydraulic system, SMC HRS090 thermochiller. Preliminary simulations show a temperature increase lower than 12.5ºC when a DC intensity current of I=400A is used.

To monitor the water flow, two flowmeters (SMC HRS-PF3W540) have been installed at the inlet and outlet of the gradient system. In addition, the flowmeter placed at the outlet of the gradient system allows the temperature to be monitored. Additionally, two pressure switches (SMC ISE20C-Y-02-W) have been installed to control the pressure in the collector system that distributes the water flow to the magnetic coils that make up the gradient system. The position of these systems is shown in **Fig.7**.

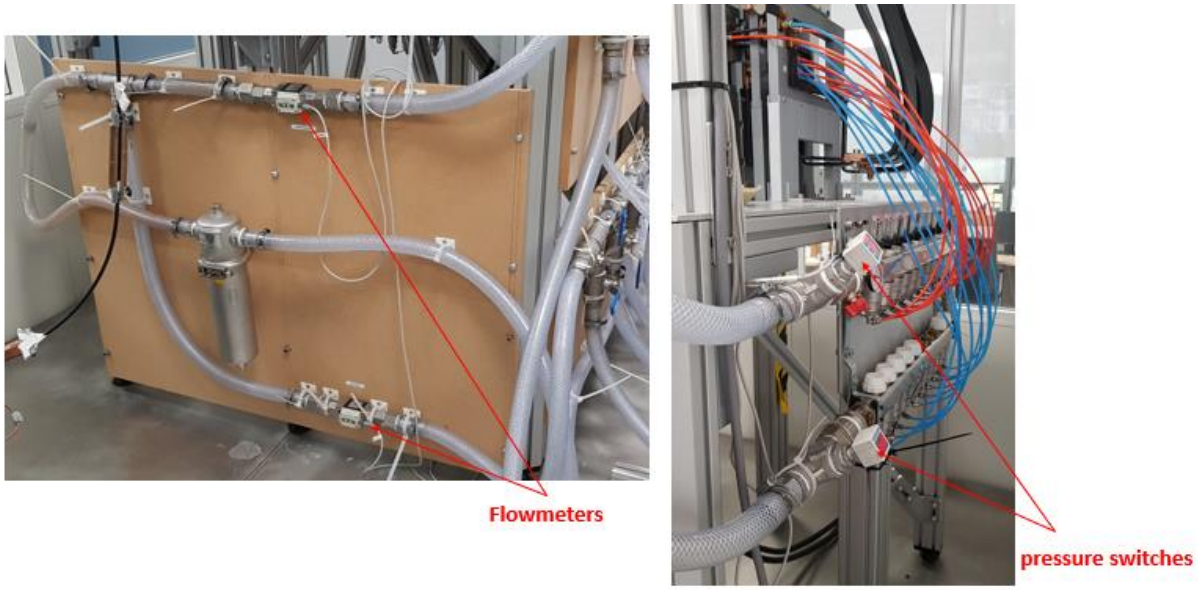

Figure 7: Diagnostic components of the gradient system.

To meet the requirements established for the gradient system, Danfysik A / S had to design and manufacturing three power supplies (PPSU, Pulsed Power Supply Unit) capable of supplying current pulses of 500 A with rise and fall times of 10 us. A picture of the first Danfysik PPSU installed in the MRILab laboratory at i3M (Valencia) and its main components is shown **Fig.8**.

Figure 8: (Right) Picture of the Danfysik PPSU. (Left) Picture of the main components.

2.1.3 Radiofrequency System.

The Radiofrequency (RF) system includes basically four different devices: RF coil, RF power amplifier, preamplifier and Tx/Rx switch.

Different configurations for RF coil were studied: saddle and solenoidal coil. Both configurations were manufactured and studied. In the end we decided to use the solenoid configuration because it was observed to have a higher SNR than the saddle configuration. The solenoidal coil has 20 turns, 15 mm od internal diameter and its length is 50 mm (see **Fig.9**). The diameter of the copper wire used is 0.4 mm. The coil is covered by an external copper shielding with rectangular prism. The holder of the RF coil and the cooper shielding are fabricated the housing with poly lactic acid (PLA) which can be easily synthetized by 3D printing and had a good mechanical resistance to support the weight of the hole subsystem. The RF coil and the sample are fit into the actuator that moves the hole system in and out the magnet, moves the sample to the appropriate position.

The RF power amplifier used is a RFPA-42-1000 from Barthel HF-Technik. AS the RF coil works as a Tx/Rx coil, we need to include in the RF electronics a Tx/Rx switch (RXTX42, Barthel HF-Technik). The purpose of the Tx/Rx switch is to protect the receiving preamplifier from the damage due to high RF power of transmit mode. Finally, we got a 50 Ohms input impedance preamplifier (LNA01, Barthel HF-Technik) to amplify the weak received signal from proton magnetic resonance. A picture of these components is shown in **Fig.10**.

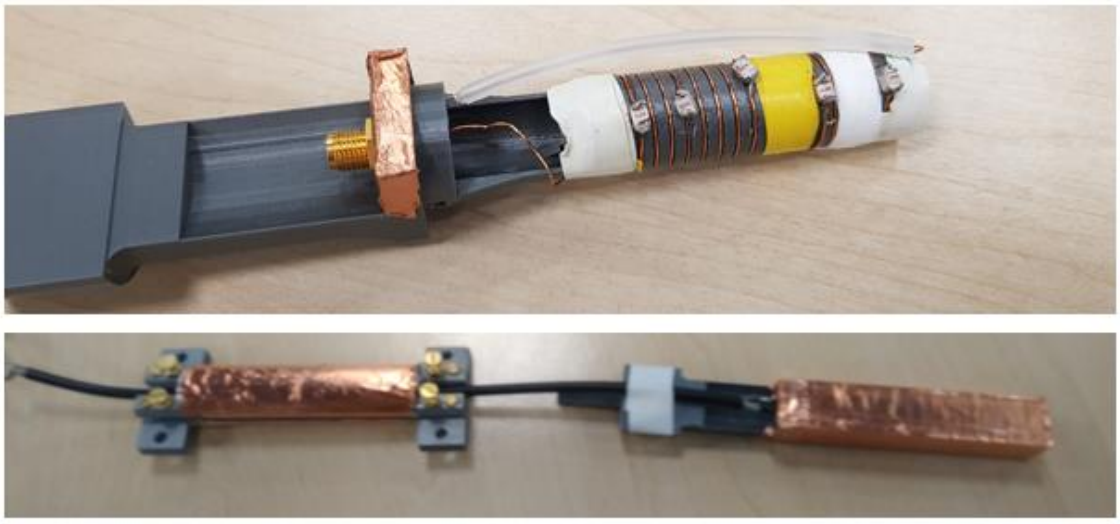

Figure 9: (Top) Picture of the solenoidal RF coil. (Bottom) Copper shielding for the RF coil.

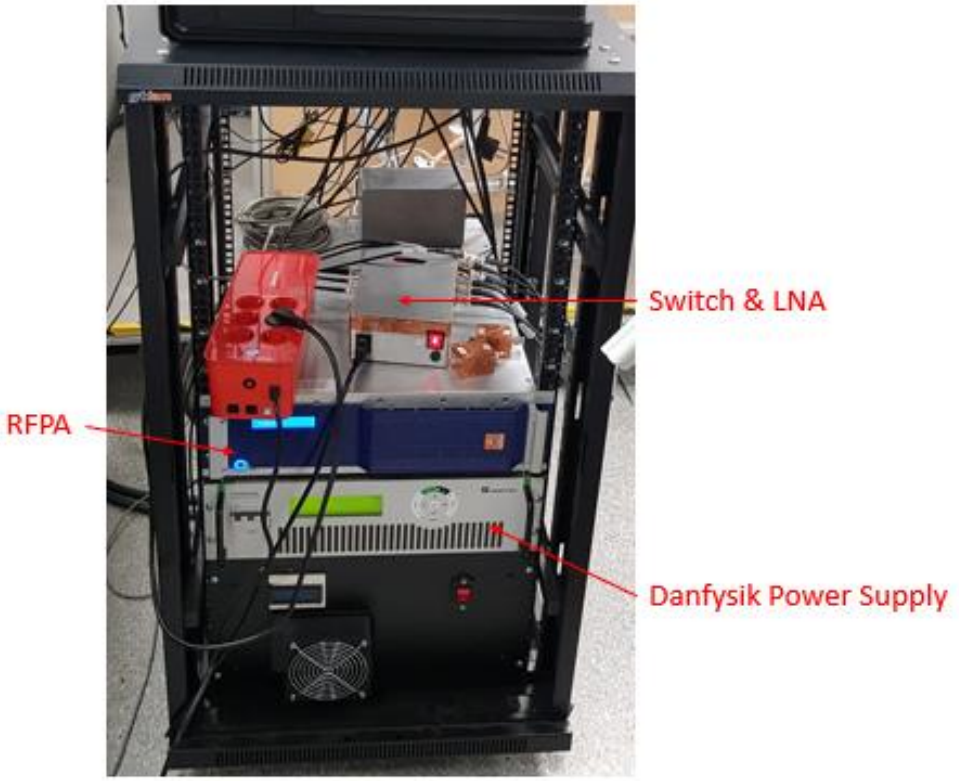

Figure 10: Picture of the radiofrequency power amplifier together with the switch and the low-noise amplifier.

A series of floating cable traps type shielded traps were designed and built that do not reduce shield currents or common mode currents along the coaxial cable. These types of traps are important because these currents affect coil tuning, image inhomogeneity and, most importantly, can cause severe burns. The floating cable trap consists of two coaxial concentric conductive cylinders, where one end is shorted together, and the other end is tuned to resonance. This cable traps have an internal and external diameter of 25 m and 70 mm respectively and 100 mm of length. These are tuned by means of a capacitor of 516 pF. A photograph of these traps and their placement on the coaxial cables is shown in **Fig.11**.

Figure 11: Picture of the floating cable trap fabricated and its placement along to the coaxial cables.

2.2 Prepolarization System.

2.2.1 Prepolarized magnet.

The experimental setup used the proof of concept of the prepolarization system in **Fig.11**. The preolarization system is composed of a main magnet, prepolarization magnet, RF (radiofrequency) coil, cooling system of the prepolarization magnet and high-power electronics. The main magnet for the offline pre-polarization setup is a C-shaped permanent magnet developed by SABR Enterprises, LLC (MA, USA). This magnet produces a maximum magnetic field of 0.26 T over a FoV (Field of View) of 150 mm diameter with homogeneity better than 20 ppm. The free space between the magnetic poles is approximately 210 mm (**Fig.12**). This setup has a planar magnetic gradient system capable of generating magnetic gradients of 0.5 T/m (400 A). The magnetic coils have been designed and manufactured by Tesoro Imaging S.L (Valencia, Spain). The magnetic gradient system (GPA-400-750) used a gradient amplifier developed by Oy International Electric Co. (Helsinki, Finland) to power the gradient coils.

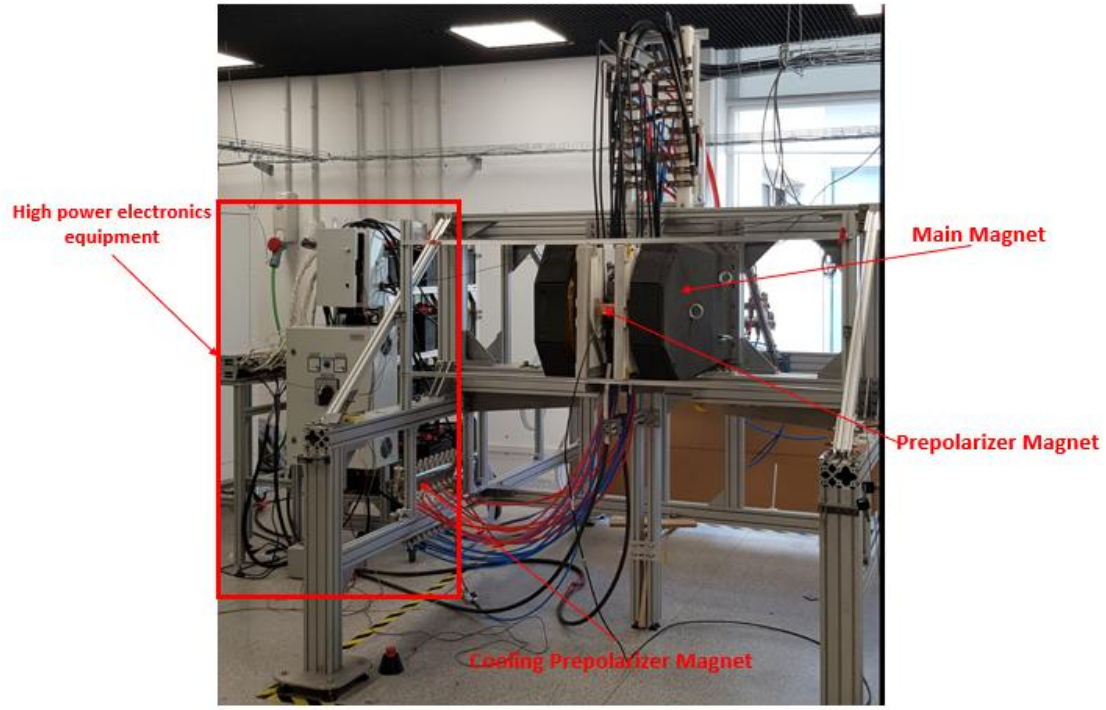

Figure 12: Experimental Setup.

The prepolarized magnet[2] consisting of ten loops, two layers per loop (spiral configuration), and sixteen turns per loop. Every layer contains two spirals of inner (outer) diameter 35 mm (99 mm), each with eight windings. The conductor we chose is hollow OF-OK copper tubing of section 4x3 mm^2 and an inner hole of 2 mm. This high purity copper is immune against hydrogen embrittlement, and the hollow section allows for water cooling. The loops are electrically connected in series and the water-cooling paths are connected in parallel to maximize heat transfer. The copper tubing is electrically isolated by a layer of fiberglass with polyester. A photograph is shown in **Fig.13**.

Figure 13: Photograph of the prepolarizer magnet.

[2] J. P. Rigla et al, A Fast 0.5T Prepolarizer Module for Preclinical Magnetic Resonance Imaging, arXiv 2103.04738, 2021.

The magnet is designed to generate a 0.48 T (B_p) magnetic field with a maximum current of 255 A. The magnetic characterization was performed with a hall probe (Metrolab THM1176-MF) attached to a 3D positioning system. The field strength profile measured along the coil axis is shown in **Fig.14 (Left)** for Ip~190A, the maximum intensity available from the Danfysik 9100 power supply employed for these tests. Thermal simulations in Comsol indicate that a water flow of ~13 l/min and a pressure drop of ~4 bar can limit the temperature increase at the coils to <13 K at a duty cycle of 100 %. To this end, we employ a water chiller (SMC HRS090-AF-40), which feeds in parallel all ten layers in the stack that forms the prepolarizer. The experimental characterization of the thermal behavior was performed at a maximum Ip of 190 A, for which a jump of 6 K (8 K) is measured at the first (last) layer (**Fig.14 Right**). The hydraulic and thermal characterization was made using a flowmeter (SMC PF3W704-F03-ETN) located at the exit of each loop.

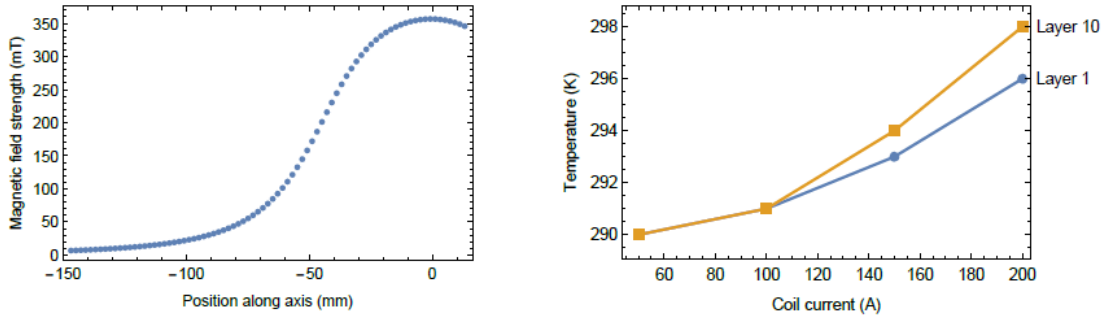

Figure 14: (Left) Magnetic-field profile measured along the x-axis for Ip _ 190 A. The zero in the abscissa corresponds roughly to the solenoid center. (Right) Temperature of the first and last layers of the prepolarizer as a function of the coil current Ip, measured after reaching thermal equilibrium.

2.2.2 Radiofrecuency System.

The RF coil used in the tests is a solenoid type coil (**Fig.15**). The coil consisted a wire loop, 13 turns of 12.75mm inner diameter and 15.1mm outer diameter and length of 42.5 mm. The cooper wire used has a diameter equal to 1.25 mm. The shielding has been built with adhesive copper with a 0.330 mm of thickness. The RF holder has been printed in 3d with PLA (polylactic acid). The coil has hollow cylinder shielding with outer diameter of 31mm and inner diameter 29mm. The electronic circuit used to tune the RF be made up of two branches, matching a tuning. The capacity used in matching is 20pF (atccncn030900, Altaix) placed in parallel trimmer (2-20PF 1000V SMD, Sprague-Goodman / SGNMA3T20009) and tuning 66pF (atccncn030800, Altaix) placed in parallel trimmer (2-20PF 1000V SMD, Sprague-Goodman / SGNMA3T20009).

The RF coil is tuned to the hydrogen resonance frequency at 0.26T (11MHz). The quality factor RF coil is 25. It was measured with the assemblies shielding and within prepolarizer by the VNA (Rohde & Schwarz FSH4 spectrum analyzer) in reflection mode (S11). This coil gets a FOV of 15mm.

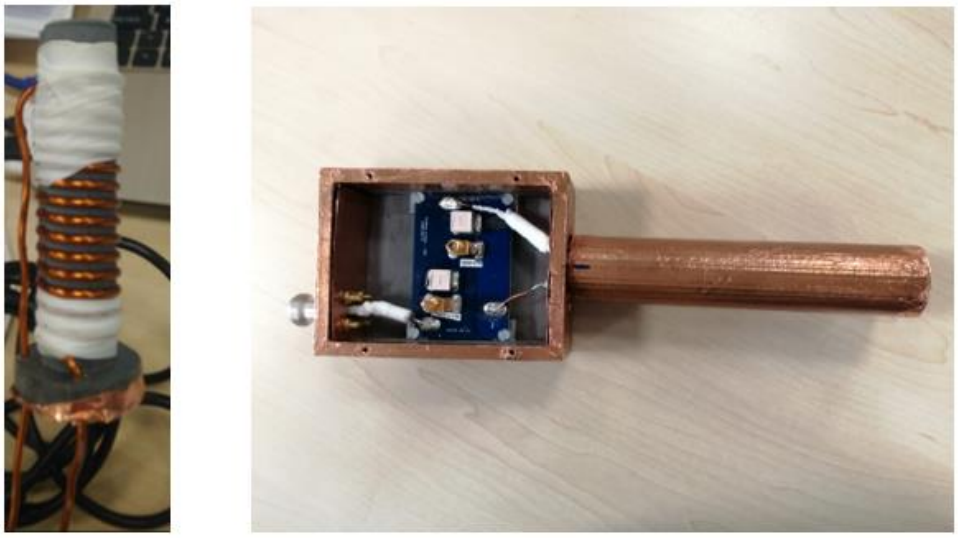

Figure 15: Pictures of RF coil used in the test.

2.2.3 Mechanical System.

The prepolarizer module is bolted to the nylon holder that accommodates the planar gradient coils of the “DentMRI - Gen I” system. As shown in the photograph in **Fig.16**, the prepolarizer coil axis is orthogonal to the main field and in the plane normal to the magnet poles, which facilitates the insertion and extraction of the rf coil and sample through the main opening of the C-shaped permanent magnet. All electrical and hydraulic connections are on the bottom. evolution magnets when the prepolarizer is on. Due to their orientation, the interaction between the magnets results in a torque on the prepolarizer module, generating a moment that points downwards. Since the prepolarization field is applied in long pulses (typically >500 ms to saturate the sample magnetization to the total field B_{tot} =(B^2_0+B^2_p)$^{1/2}$~0.55 T), the mechanical stress is also pulsed.

This is problematic if the prepolarizer is not tightly fixed, since the whole module (including the rf coil and the sample) shifts to a different place during the application of the prepolarization field, and the sudden return to its relaxed position results in sample motion which compromises the quality of MR images. To address this, we have 3D-printed and installed several adjustable spacers which press against the inner surfaces of the prepolarizer and gradient coil holders (see **Fig.16**). In this way, we suppress mechanical motion to the point where we cannot observe any influence on the detected rf signals.

Another relevant aspect is to prevent noise present in the laboratory (or generated by our electronics) from being picked up by the prepolarizer electrical connections and affecting the weak rf signal which we use for image reconstruction in MRI. To this end, scanners invariably use Faraday isolating cages around the resonant detection coils. With the prepolarizer module installed, the Faraday cage is inside the prepolarizer, directly around the small rf coil, which is coaxial to the prepolarization module. We found this necessary but insufficient when the thick cables from the IPM-16P outputs are connected to the prepolarizer load. This was solved by shielding the cables and connecting them to the RF ground. For reference, **Fig.17** shows a Free Induction Decay (FID) curve when unshielded.

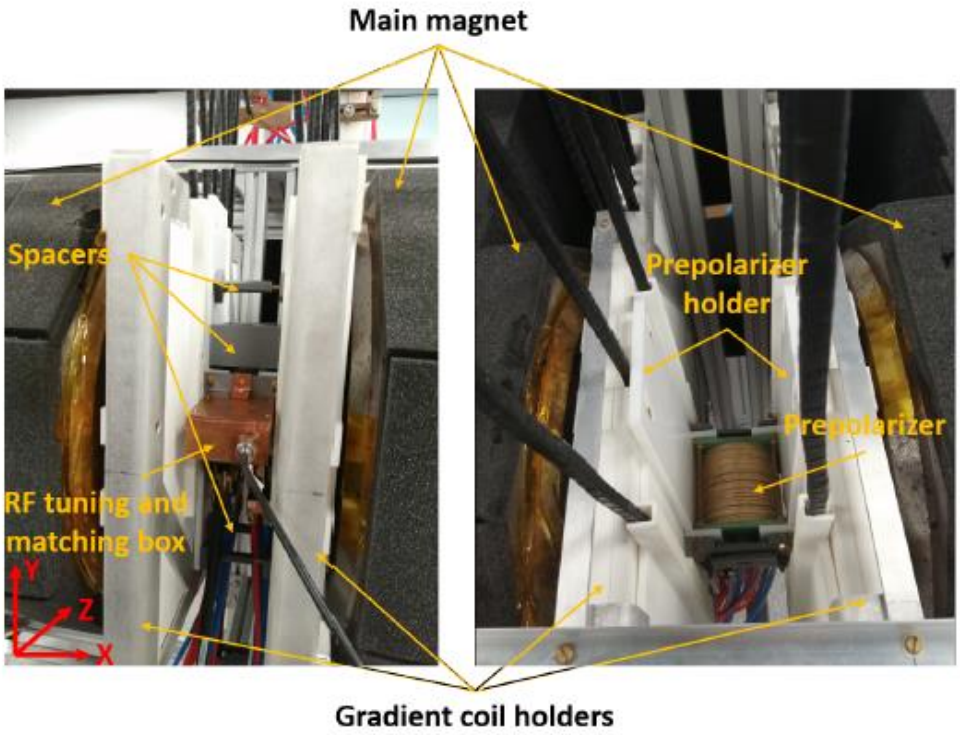

Figure 16: Front (left photograph) and top (right photograph) views of the prepolarizer module after installation in the "DentMRI - Gen I" scanner. The front view shows the spacers used for mechanical stability (see text), as well as a box containing tuning and matching electronics between the high power rf amplifier and the resonant coil. The prepolarizer magnet and holder are best viewed on the right photograph, which was taken right after the module was installed.

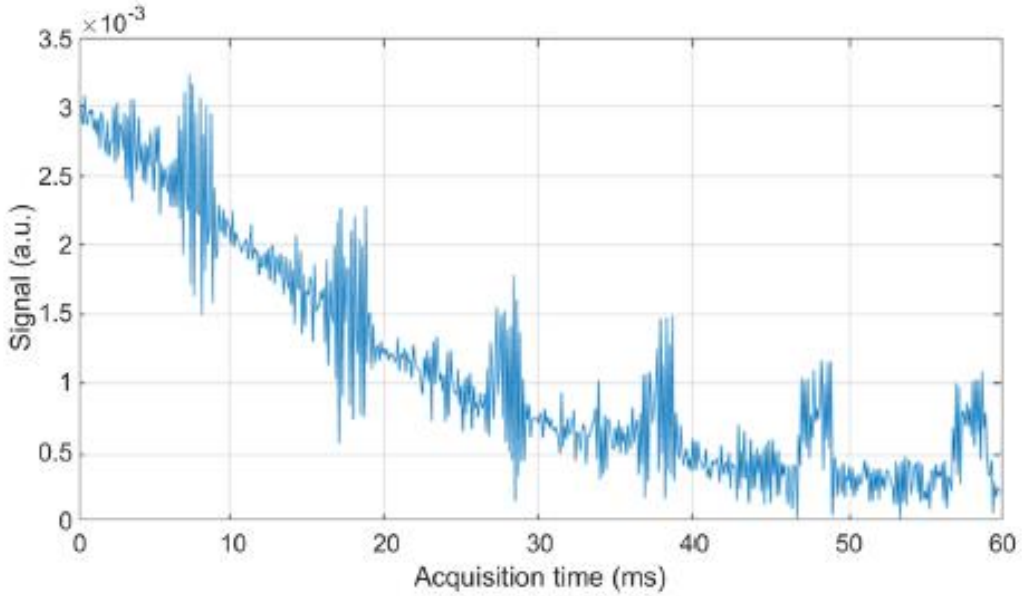

Figure 17: Free Induction Decay (FID) of a mouse brain sample before rf grounding of the prepolarizer cables' shielding. The overall noise level decreases significantly after proper grounding, and the periodic bursts every 10 ms (presumably the second harmonic from the 50 Hz network) disappear.

2.2.4 High-Power Electronic System.

To test the concept of the proposed prepolarization system, we design and build a high-power electronic system for demonstrating PMRI of softer tissues, which is less demanding in term of the switch off time τ. The high-power electronics equipment present in the laboratory is shown in **Fig.18**.

This setup relies on a high-power switching module (IPM-16P from Eagle Harbor Technologies Inc.)[3] based on 16 Insulated-Gate Bipolar Transistors (IGBTs). Each of these can take 1,200 V and 80 A, for a total device current of 1,280 A. However, the IPM-16P is driven from a battery bank consisting of 16 commercial batteries (12 V, LFS 105N from Varta Automotive)[4]. For our total load resistance of ~95mΩ (~75mΩ from the coil, ~20mΩ from cables and connections), every battery output a current ~128A when fully charged. We therefore arrange the batteries in pairs, each pair with both batteries connected in series. To prolong the batteries' discharge time, we use all 8 pairs simultaneously, connected in parallel.

The positive end of every pair is connected through a diode (VS-70HF40)[5] to a thick copper plate that serves as the positive input of a custom-built high-power connection box (see **Fig.18 (b)**). This is then connected to a second copper plate (positive output from the connections box) through a relay (Kilovac LEV200)[6], enabled by a manual stop button and an interlock to ensure the prepolarizer is never charged if the water chiller is not functional. The negative ends of the battery pairs are similarly connected (without diodes) to the bottom copper plate, which serves as both negative input and output. The IPM-16P outputs are connected to the prepolarizer with cables of section 95mm^2, which we shield with a conducting mesh (Scotch electrical shielding tape 24). This mesh is grounded through the radio-frequency (rf) shield of the resonant coil used for coherent spin manipulation and resonant MRI signal detection. This strongly suppresses rf noise pickup and 50 Hz inductive couplings which otherwise strongly deteriorate our MRI signals.

The control system is based on a RadioProcessor-G console from SpinCore Technologies[7]. To control the prepolarizer via the console, we use a TTL line which triggers the IPM-16Pswitches after optical decoupling in the FT1 module (Eagle Harbor Technologies Inc.).

An inductive probe for current measurement (Danisense DS600ID)[8], which we use to monitor the system's performance and characterize the prepolarizing pulse properties. The only high-power active element in the system is the IPM-16P module, so the on-off transitions at the coil are voltage controlled and the current intensity shows an exponential (rather than linear) behavior, with an expected time constant ~6.4 ms when a battery pair delivers 24 V. A complete diagram of the high-power electronics system is shown in **Fig.19**.

The structure of the measured pulses can be seen in **Fig.20** and is consistent with the above expectations.

[3] https://www.eagleharbortech.com/product-categories/solid-state-switch-modules/high-power-solid-state-switches/
[4] https://www.varta-automotive.com/en-gb/products/varta-professional-dual-purpose/930-231-115
[5] https://www.newark.com/vishay/vs-70hf40/standard-diode-70a-400v-do-203ab/dp/09F7335
[6] https://www.digikey.com/catalog/en/partgroup/lev200-kilovac-series/901
[7] J. M. Algarin, E. Diaz-Caballero, J. Borreguero, F. Galve, D. Grau-Ruiz, J. P. Rigla, R. Bosch, J. M. Gonzalez, E. Pallas, M. Corberan, C. Gramage, S. Aja-Fernandez, A. Rios, J. M. Benlloch, and J. Alonso, "Simultaneous imaging of hard and soft biological tissues in a low-field dental MRI scanner," *Scientific Reports*, vol. 10, no. 1, p. 21470, 2020. [Online]. Available: https://doi.org/10.1038/s41598-020-78456-2
[8] Danisense DS600ID: https://www.danisense.com/images/pdf/0-600A/DS600ID.pdf

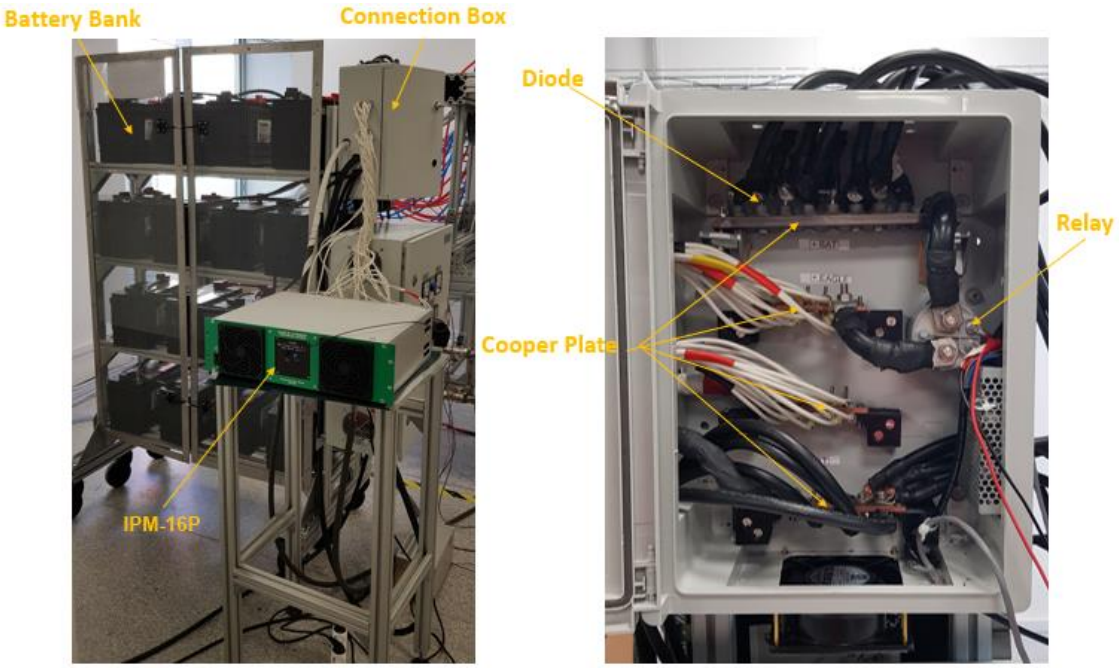

Figure 18: (a) High power electronics equipment used for demonstrating PMRI, including the IPM-16P for high power switching, the battery bank and connection box for supplying the IPM-16P. (b) A photograph of the inside of the connection box is also shown for reference.

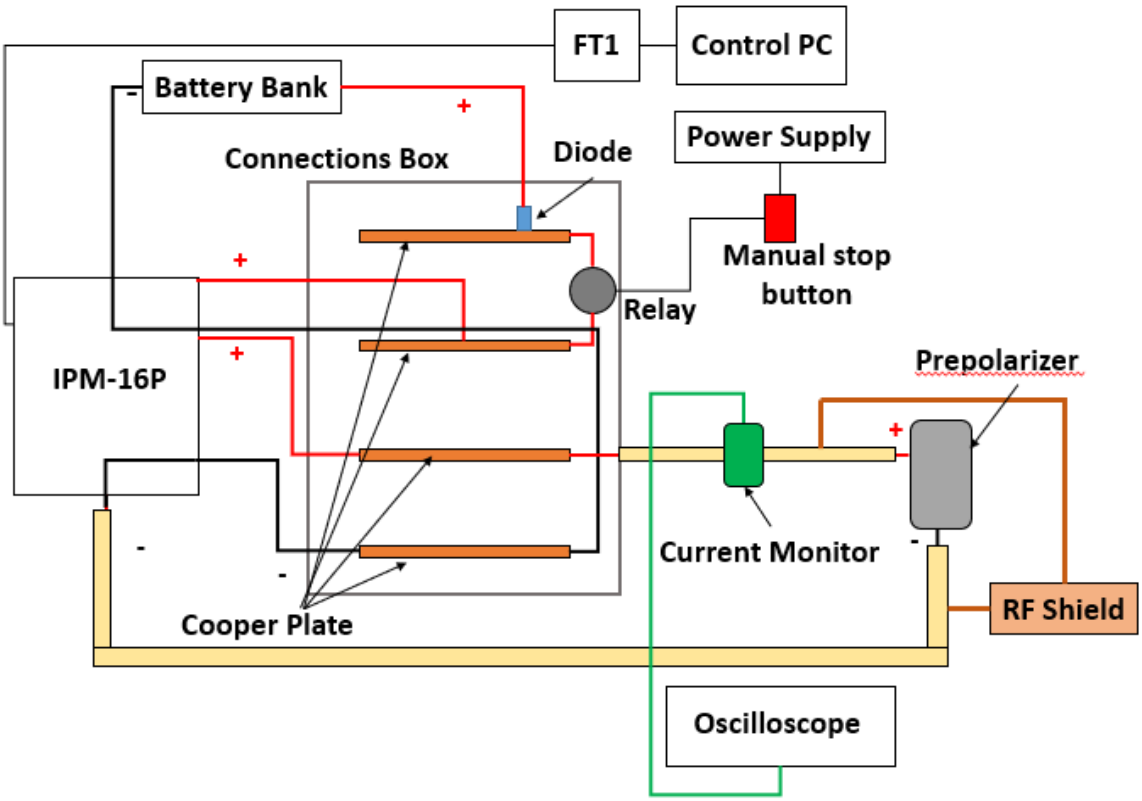

Figure 19: High-power electronic system.

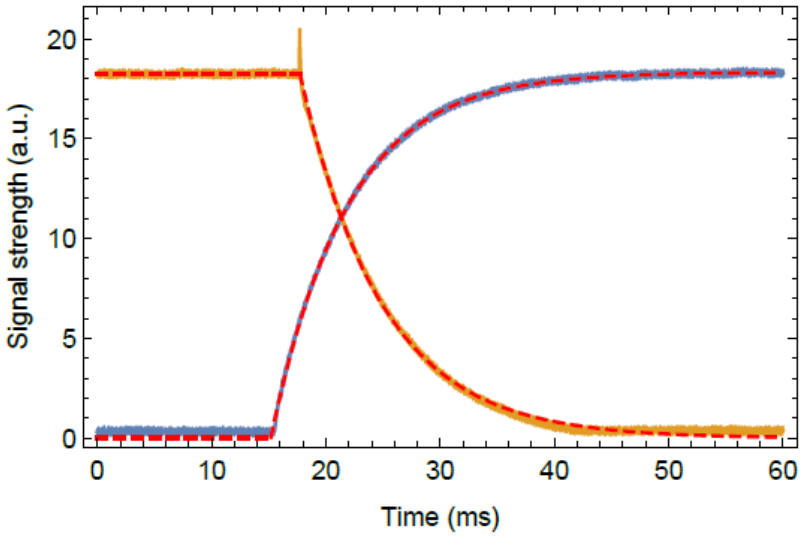

Figure 20: Oscilloscope traces corresponding to the exponential rising and falling edges for the current pulsed through the prepolarizer when driven with the IPM-16P and battery bank. The coil current in this example is Ip~255A. The red dashed lines are fits to simple exponential functions, yielding τ ~6.7 ms (7.2 ms) for the rising (falling) edge, consistent with expectations (see text). The spike right before the rising edge is a fast transient due to the switching electronics in the IPM-16P.

2.2.5 Prepolarized Test.

To test the performance of the prepolarizer module and his effect on raw MRN signals, we introduce initially tap water as a sample due to its long-lived signal. We have measured the T_1 of tap water to be ≈ 1.87 s using an Inversion Recovery sequence. We run a first set of measurements consisting in two pulses: a prepolarization pulse of variable length and 0.55 T strength followed by a $\pi/2$ resonant RF pulse to coherently rotate the prepolarized sample magnetization. These are repeated for three different wait time between pulses: 30 ms, 50 ms and 100 ms. The choice of this dead time compromises the effect of remanent current flowing in prepolarizer when the RF pulse is transmited, which otherwise shifts the Larmor frequency and distorts the FID signal due to its intrinsic inhomogeneity. Then, the FID is acquired during 40 ms after the RF pulse after waiting 80 us for the coil ring-down to fade away. **Figure 21** shows the absolute value of the FIDs (after quadrature demodulation at ω_0) for different prepolarization pulses (going from 0.5 s to 4 s, enough to saturate completely magnetization) for a dead time of 30 ms. As can be seen in this figure, when the prepolarization time increases, an increase in the FIDs is observed.

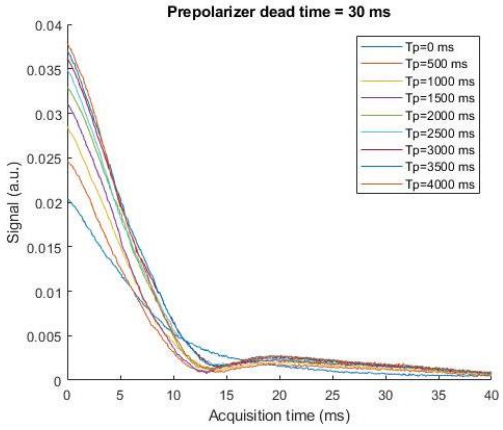

Figure 21: Comparative dataset of prepolarized FIDs for tap water as a function of the prepolarization time tp, for t_{dead} = 30ms and B_{tot} ≈ 0.55 T.

3 Diagnostic and Interlock System.

3.1. HISTO-MRI diagnostic and interlock system.

As described in this document, a diagnostic system has been installed in the HISTO-MRI scanner consisting of a series of flowmeters and pressure switches to control the water flow (4 SMC HRS-PF3W540) and water pressure (2 SMC ISE20C-Y-02-W) of the main magnet and the magnetic gradient system cooling systems, respectively. To monitor all the data supplied by the different components of the diagnostic system, a GUI in LabView was developed (**Fig.21**). Through this Grafical User Interface (GUI), it is possible to monitor the data supplied by all the components of the diagnostic system in real-time, as well as to store all the data in a file for later analysis. Communication between the different components of the diagnostic system and the control PC is done through a USB 16-Bit High-Speed Multifunction DAQ Devices (Measurement Computing Corporation, USA)[9].

In this GUI we include the control of the main magnet power supply (**red square Fig.22**), allowing to turn on / off the power supply and controlling the supplied current. Besides, we include the control of the main magnet (**blue box Fig.22**) and the gradient system chiller (**green square Fig.22**) thermo-chillers. From the GUI the thermo-chillers can be switched on and off, as well as controlling the cooling water outlet temperature.

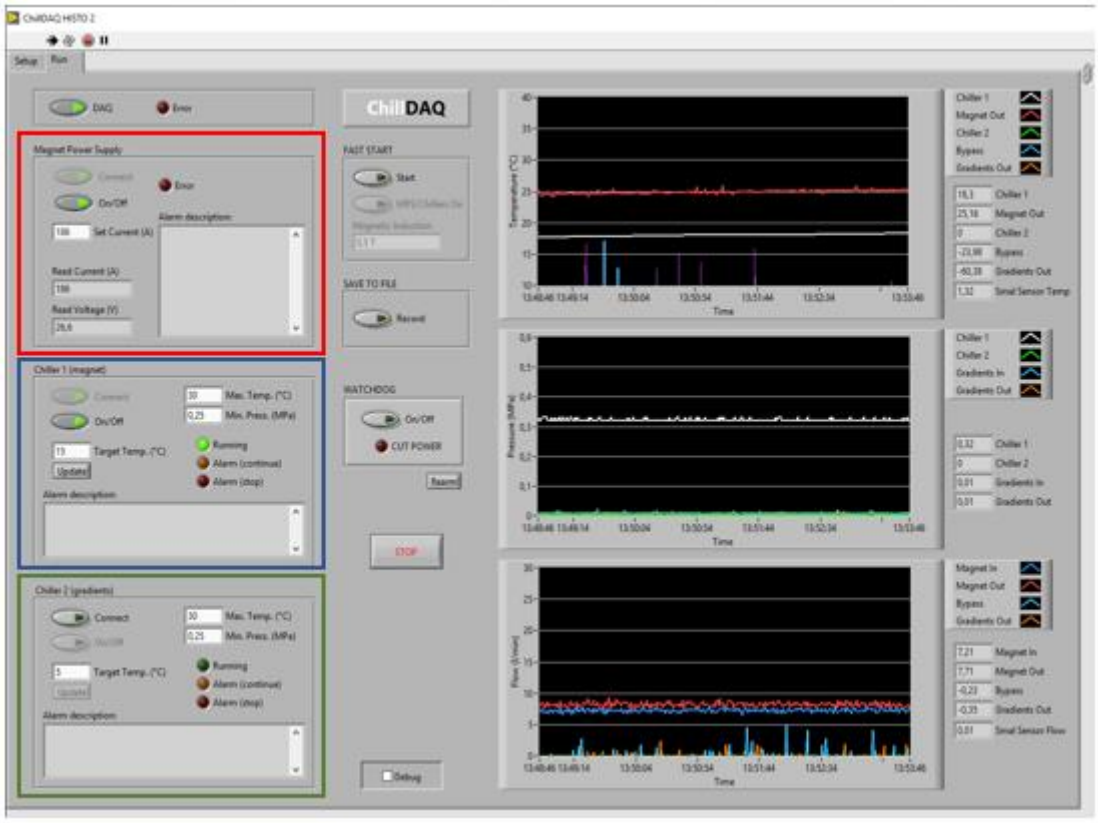

Figure 22: GUI of the diagnostic system for HISTO-MRI system.

To avoid damage to the HISTO-MRI scanner due to the non-correct operation of some of its components (Main magnet and gradient system), an interlock system was implemented. This interlock system cuts the current output of the Danfysik power supply of the main magnet. If the system detects an abnormal value in any of the established parameters (Temperature, flow and

[9] https://www.mccdaq.com/usb-data-acquisition/USB-1608G-Series.aspx

pressure) of the cooling system: excessive increase in the temperature of the cooling water, drop in water flow and / or pressure system. In addition, an automatic power cut prompt appears in the GUI of the diagnostic system.

3.2. Prepolarization diagnostic system.

For the Prepolarization System a GUI based on Labview was developed. This GUI allows monitoring in real time the charge level of the battery bank. In the same way, we observed the current pulses at the input of the prepolarization magnet can be observed using an inductive probe Danisense DS600ID.

4. Summary.

All the components that are part of the HISTO-MRI scanner (main magnet, gradient and RF systems) as well as the different subsystems of these components (cooling system, diagnostic system…) have been manufactured and integrated together. In addition, these systems have been found to work as expected.

The pre-polarization system (prepolarized magnet, RF system, high-power electronics, diagnostic system and cooling system) has been designed and manufactured. This system has been integrated into a low-field MRI scanner in which we have verified the correct operation of the prepolarization system.